# Methods for Developing ASF Grids for Harbor Entrance and Approach

Dr. Peter Swaszek; **University of Rhode Island**
Dr. Gregory Johnson, Christian Oates, Mark Wiggins; **Alion Science & Technology**
CAPT Richard Hartnett, PhD; **U.S. Coast Guard Academy**

## Abstract

Much effort has been expended over the years to mitigate the effects of ASF on Loran position accuracy; primarily by trying to estimate the ASF (per Loran signal) and remove it before implementing the Loran position solution. This paper considers ASF estimation appropriate for the harbor entrance and approach application. The current thinking in the Loran research community is that the tight error requirement for this application demands the use of dense ASF grids on the harbor area. Here, we show the results of ASF data collection in New York harbor during 2006 and methods for developing ASF grids capable of meeting the HEA accuracy requirement.

## Introduction

The position solution available from the standard Loran system, while highly repeatable, suffers from poor absolute accuracy, particularly when compared to GPS. The primary reason for this is something called Additional Secondary Factors (ASFs) which are additional time delays in the propagation of the Loran signal between the Loran station and the user's receiver over that experienced along an all seawater path [1]. Common causes of ASFs include varying ground conductivity, topography, and weather. For the application of Harbor Entrance and Approach (HEA), these ASFs are particularly bothersome due to the tight accuracy requirements desired (under 20 meters position error, 2 sigma variation).

The current thinking in the Loran research community is that Enhanced Loran (*e*-Loran) will achieve this required level of position accuracy by removing the ASFs from the Loran signal time-of-arrival data before the position solution. Typically, we think of the ASF as consisting of two components:

- a temporal term (possibly with strong diurnal and seasonal characteristics) – it is envisioned that this component (or at least a large part of it) is removed by subtracting out the equivalent temporal term measured at a nearby Loran monitor site and broadcast over the Loran Data Channel (LDC). Current research issues on this approach include the correlation distance of the monitor site, methods for "smoothing" the ASF measurements at the monitors, and how to combine temporal terms from multiple monitors (see our companion paper in this proceedings, [2]).
- a spatial term – it is envisioned that this component is tabulated as an ASF "grid" that is interpolated (possibly in a bootstrapping, iterative way as discussed in [3]) to identify the value for removal.

The methodology necessary to generate this ASF grid is, then, a primary issue for HEA navigation; and it is the subject of this paper. We begin with a review of a recent ASF data collection effort in New York harbor during 2006; this consists of both static (receiver held fixed in location) and dynamic (receiver moving) data. We review the processing of this data to yield

valid ASF values. We then examine various approaches to generating the ASF grids, including a review of our previous efforts.

## Data Collection in NY Harbor

During 2006 we twice collected Loran data in New York harbor. In both cases a vessel was equipped with our standard "data collection" unit consisting of a Loran receiver (outputting TOAs for all observable Loran stations), a GPS receiver (to provide position truth), a stable clock (for precise time referencing), and a laptop PC for logging data. The first collection effort employed both a ship and the FAA test van (shown in Figure 1); the second collection effort was by ship only (shown in Figure 2).

**Figure 1 – Data collection ship (Launch #5) and van.**


**Figure 2 – Vessel used in Phase II data collection, the Jeanne II.**

To collect reference data (so as to be able to subtract any temporal variation in the ASFs), we simultaneously set up an ASF monitor site at Fort Wadsworth, on Staten Island (a Locus LRSIIID with E-field antenna). This was set up temporarily for the Phase I data collection but then made into a long-term seasonal monitor site prior to the Phase II data collection. Our parallel paper in this proceedings [2], describes the monitor site equipment configuration. Figure 3 shows the antenna mount at that site and our technical support expert, Mark Wiggins, hard at work.

**Figure 3 – Temporal monitor site on Staten Island.**

The first data collection effort was in May 2006. The on-the-water portion consisted of a slow circuit of the harbor (at 5-6 knots) and measurements at 25 static locations; the on-the-land component consisted of 19 static locations. Figure 4 shows the relative locations of the static points, all around the upper harbor region (north of the Verrazano Bridge); Figure 5 shows the track of the slow circuit, mostly contained within the upper harbor (blue) with one trip outside the harbor on a second day of measurements (green). For reference, the directions to the 4 primary Loran stations are shown in this figure.

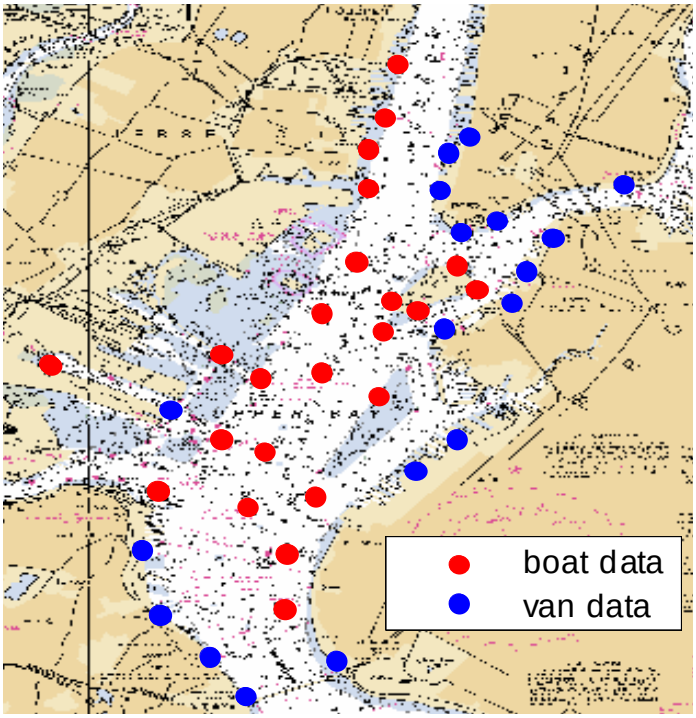


**Figure 4 – Phase I static data sites.**

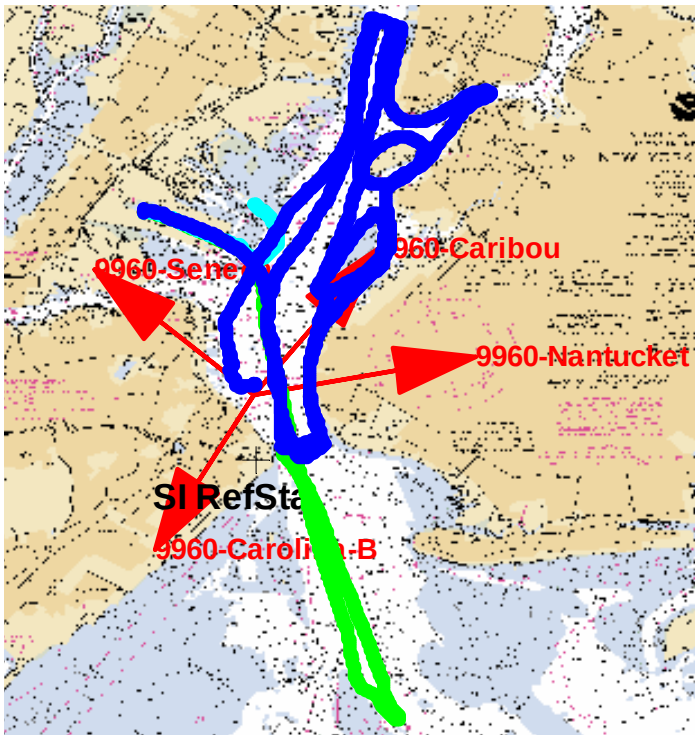


**Figure 5 – Phase I dynamic data collection tracks.**

The second data collection effort occurred in August 2006. It included 12 static locations in the lower harbor (shown in Figure 6), repeated the circuit of the upper harbor from Phase I, and added slow cruises in the lower harbor. The Phase II tracks are shown in Figure 7 (the three distinct colors show the tracks from three different days of measurements).

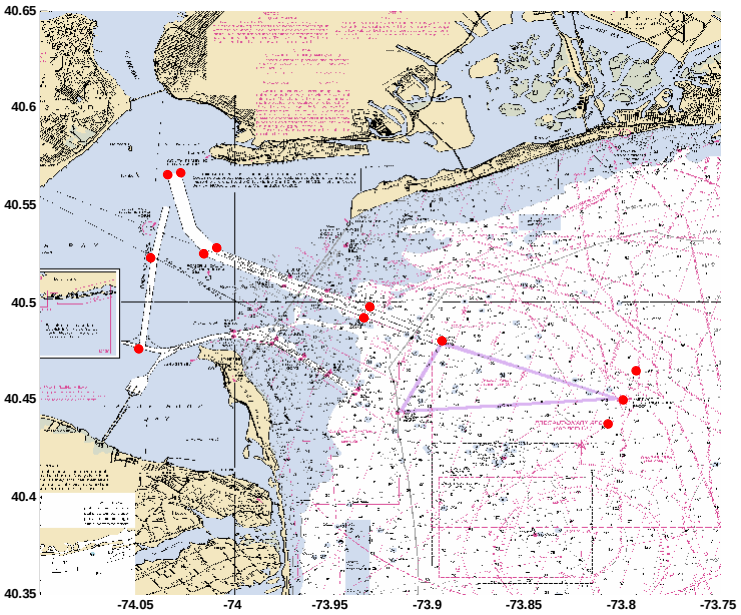


**Figure 6 – Phase II static data sites.**

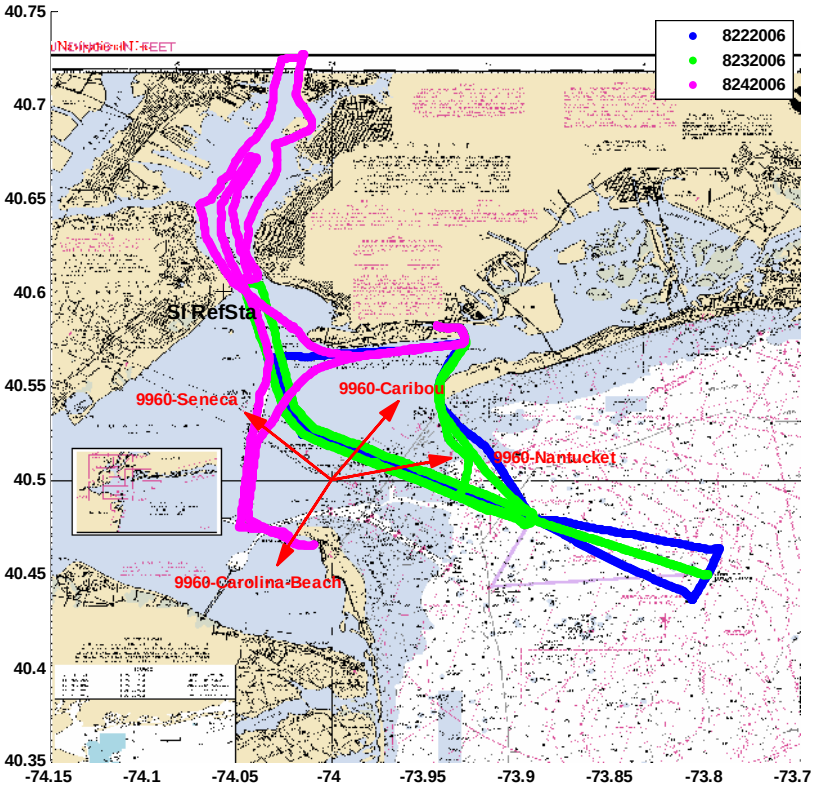


**Figure 7– Phase II data collection tracks.**

The collected data (both static and dynamic) was post-processed to produce ASFs as follows:

- First, the dynamic Loran TOAs are inverse filtered to remove the effects of vessel movement during the receiver averaging[1].
- Precise location for each data point is computed from the L1/L2 GPS pseudorange data with GrafNav software using data from the local CORS sites. The expected TOA is computed from this precise position (taking into account primary and secondary Loran factors).
- The ASFs are calculated as the difference between the expected TOA and the inverse filtered TOAs.
- Relative ASFs are calculated by removing the measured ASF at the Staten Island reference site ($ASF_{rel} = ASF_{boat} - ASF_{SI}$).

Figure 8 shows typical ASF data resulting from this computation on the Phase II data for Loran station Nantucket. In this figure we see relative ASFs (again, relative to the value at the monitor

[1] This inverse filtering technique has been in use by the authors for over a year and although mentioned in our ILA 34 paper [4] it has not been previously documented. We analyzed the Locus Loran receivers used in our ASF measurement system and developed a model of the filtering done by the receiver. We then apply an inverse of this filter model to remove the receiver averaging and time lag.

site) ranging from –1 to +0.7 µsec depending upon the ship's position in the harbor. (The ASF is negative relative to the monitor site in the southern outer harbor area since the path from Nantucket to the ship is all seawater while the path to the monitor site travels partially over Long Island. At the northern end of the harbor, the additional land path of southern New England, when compared to the monitor site, results in positive ASFs.)

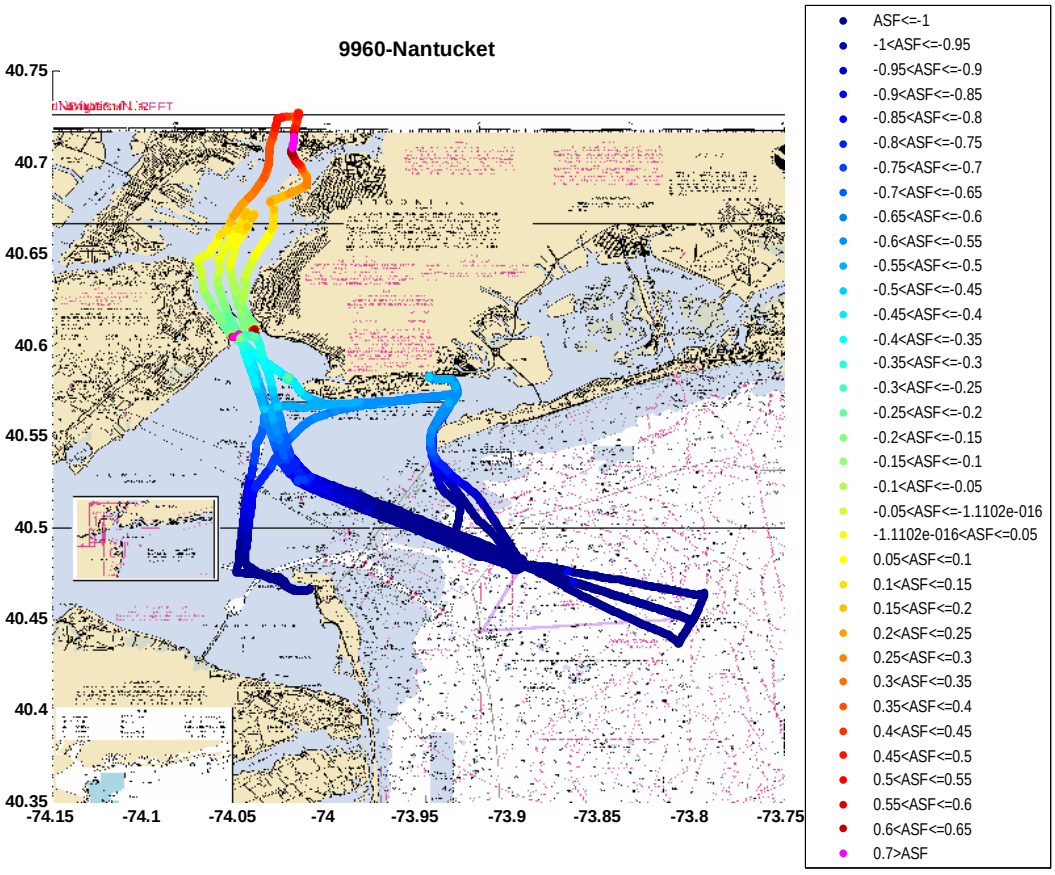


**Figure 8 – Typical relative ASF measurements.**

# Grid Development

In prior work, we have considered the generation of harbor ASF grids. Our first attempt [3] was to employ the BALOR software to predict ASFs on the Thames River in Connecticut (adjacent to the Coast Guard Academy) and to experiment with the resolution required to achieve HEA levels of accuracy. To do so, we first generated a very dense grid from the modeling software; a typical example is shown in Figure 9 for Loran station Nantucket. We then considered varying amounts of subsampling of this grid (and then interpolating back) to observe its effect on Loran performance. Figure 6 of that paper (reprinted below as Figure 10) shows the theoretical position performance (95%) versus grid point spacing. The conclusion was that a grid with approximately 500 meter spacing should meet the HEA accuracy requirements. A typical coarse grid from this early work is shown in Figure 11. Unfortunately, the original BALOR predictions of the ASFs are insufficiently close to the true ASFs to make this method of developing the ASF grid reliable.

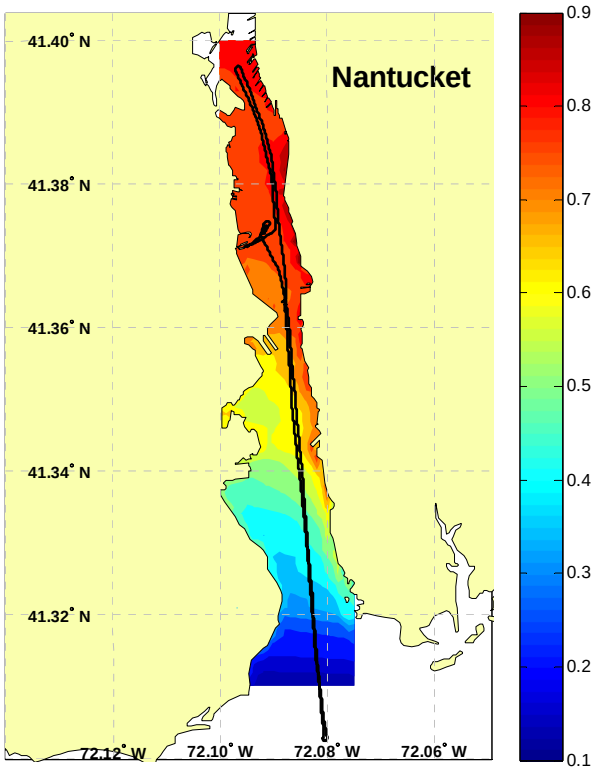


**Figure 9 – ASF prediction on the Thames River using BALOR (from [3]).**

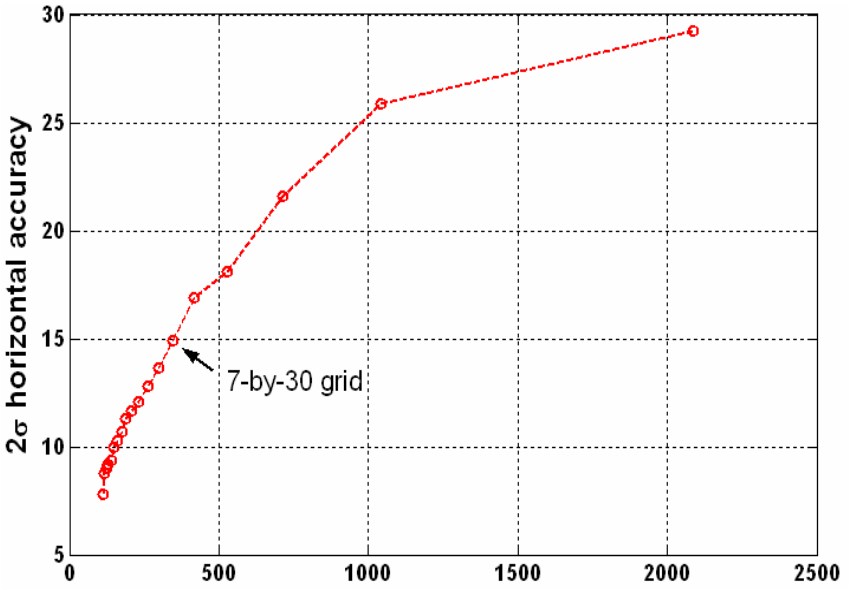


**Figure 10 – Theoretical Loran position performance versus grid spacing (from [3]).**

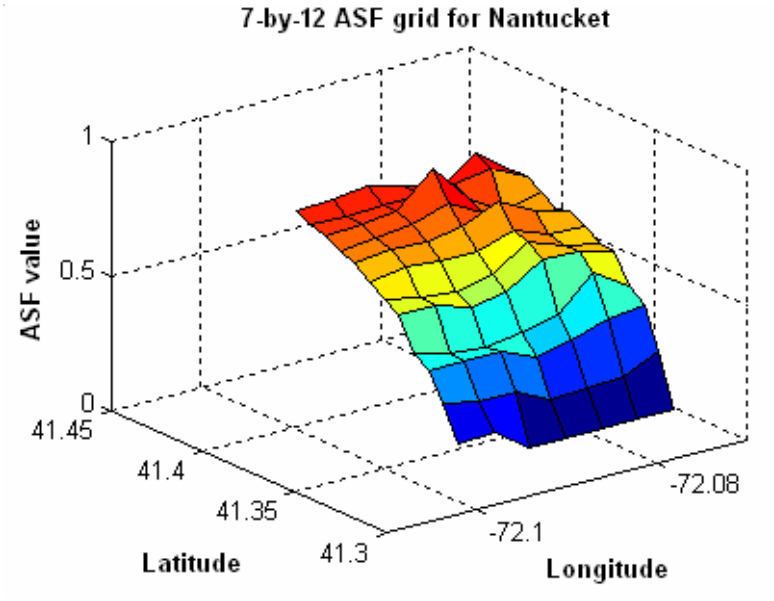


**Figure 11 – A typical ASF grid (from [3]).**

Since the BALOR predictions were seen as not being accurate enough, we turned to collecting and processing on-the-water data. In a second attempt at grid generation, we collected actual ASF data while slowly cruising on the Thames River, converting the data into ASF grids (at this point we did not employ a reference station; otherwise, the data collection effort was similar to that reported above). The results of this work were presented in [5]. The grid was generated as follows:

- A priori, we located a 7-by-12 point grid on the river as shown by the red dots in Figure 12 (reprinted from [5]). A second component of our prior work [3] suggested that such a grid size might be sufficient for the Thames River scenario.
- We grouped data points to the nearest grid point. The color coding of the tracks in Figure 12 attempts to show these groupings. For example, the red swath of track at the bottom right maps to the bottom right grid point; moving left, the green swath maps to the bottom row of the grid, second point from the right; etc. This mapping is better seen in Figure 13, a blow-up of a portion of Figure 12 (also reprinted from [5]).
- The grid value is chosen as the median of the data points mapped to it. The median was chosen, instead of the mean, to limit the effects of outliers.

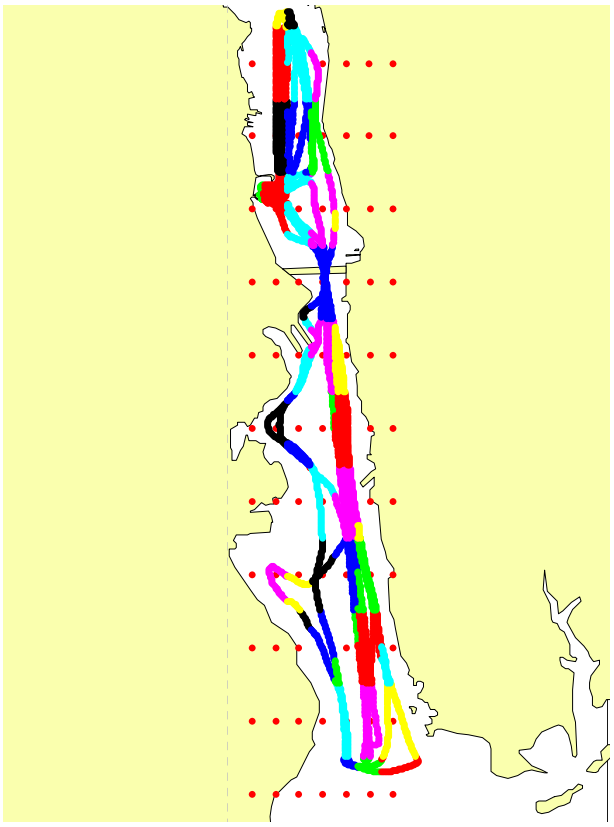

**Figure 12 – The 7-by-12 grid for the Thames River (from [5]).**

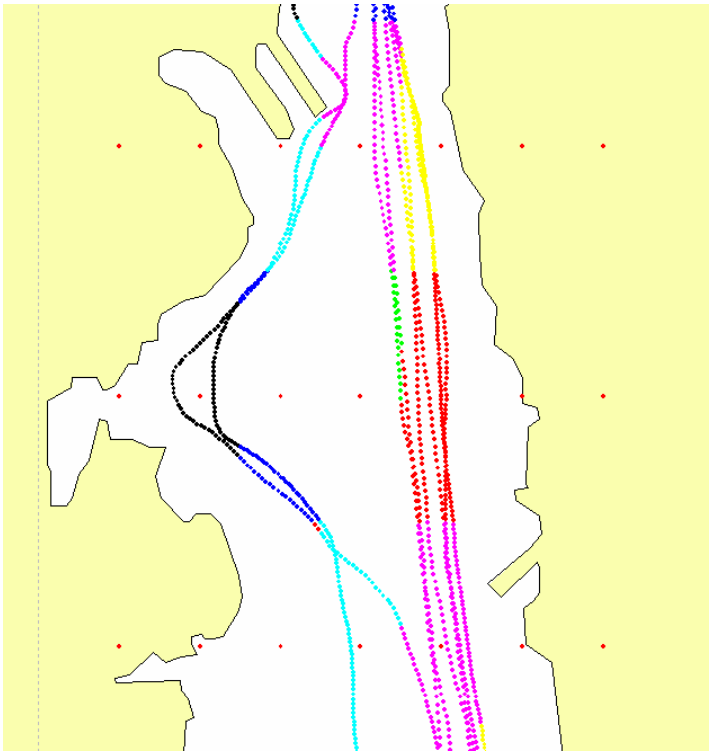

**Figure 13 – A blow-up showing the Thames River mapping (from [5]).**

While this simple process yielded better grids than those developed from the BALOR model, the process still suffered from multiple limitations:

- Some ASF grid values are missing – an example is the grid point in the left of center of Figure 13. This is, of course, due to no data being mapped to the grid points; while this is expected of land points, it's disappointing for on-the-water grid locations.
- There is no explicit correlation of ASF value at adjacent grid points. While we expect the ASF to be a smoothly (continuously) varying function of spatial position, our naïve mapping/median computation does not explicitly create this correlation.
- The relative geometry of the data (i.e. its position relative to the grid point) once it is mapped to a grid point is not used in any way. While we would hope that data measurements are made uniformly on the region mapping to a grid point, this is almost never the case in practice. Typically, the data is strongly biased. For example, the yellow data points on the top, right of center portion of Figure 13 map to the grid point to the right of all of that data.

Our current work seeks to mitigate these limitations. Before we get to the final results, we show a possible method using static measurements.

## *Grid Creation – Static Data*

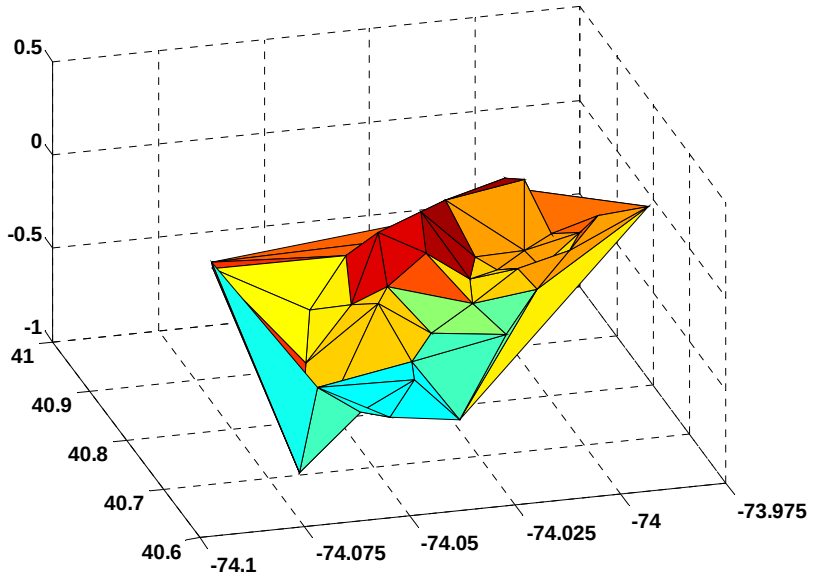


**Figure 14 – Delaunay triangle ASF surface for Nantucket.**

Referring back to Figure 4, we have data collected at multiple on-land and on-water sites in the New York harbor area. First, we average the data to remove noise. At that point, a standard interpolation method is to create a series of flats on the triangles connecting adjacent points (so called Delaunay triangles). As an example, the result using the Nantucket component of our measured data appears in Figure 14. As this non-regular surface is difficult to interpret, we resample it to a uniform 0.005 degree spacing in latitude and longitude (approximately 500 meter spacing in the New York area); the Nantucket example of this easier to digest ASF surface plot appears in Figure 15. The coverage of this result on New York harbor is shown in Figure 16 in

which the light blue points show the full grid considered (a 25-by-31 uniform 0.005 degree grid); the dark blue points are those for which we were able to interpolate data. (Another possible option for static data that we have explored, but have no results on, is to apply universal kriging [6] to the data.)

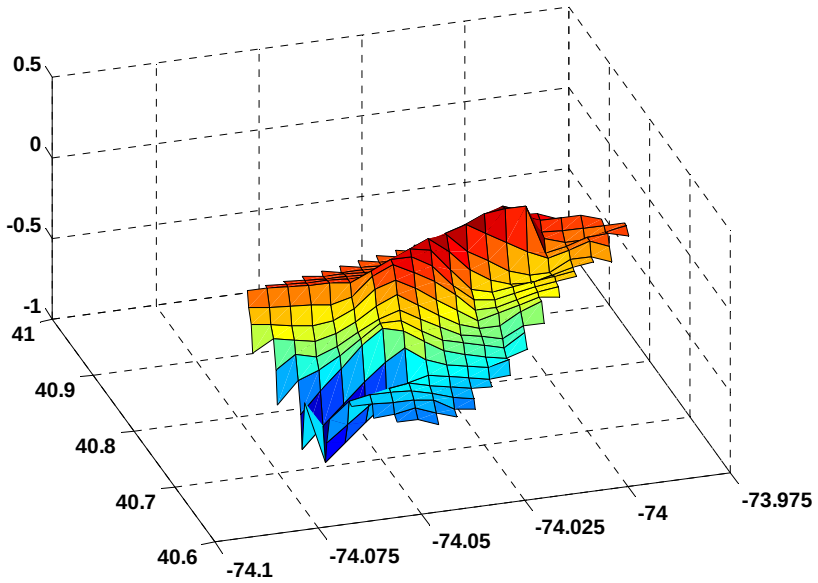


**Figure 15 – Uniform resampling of the Delaunay ASF surface for Nantucket.**

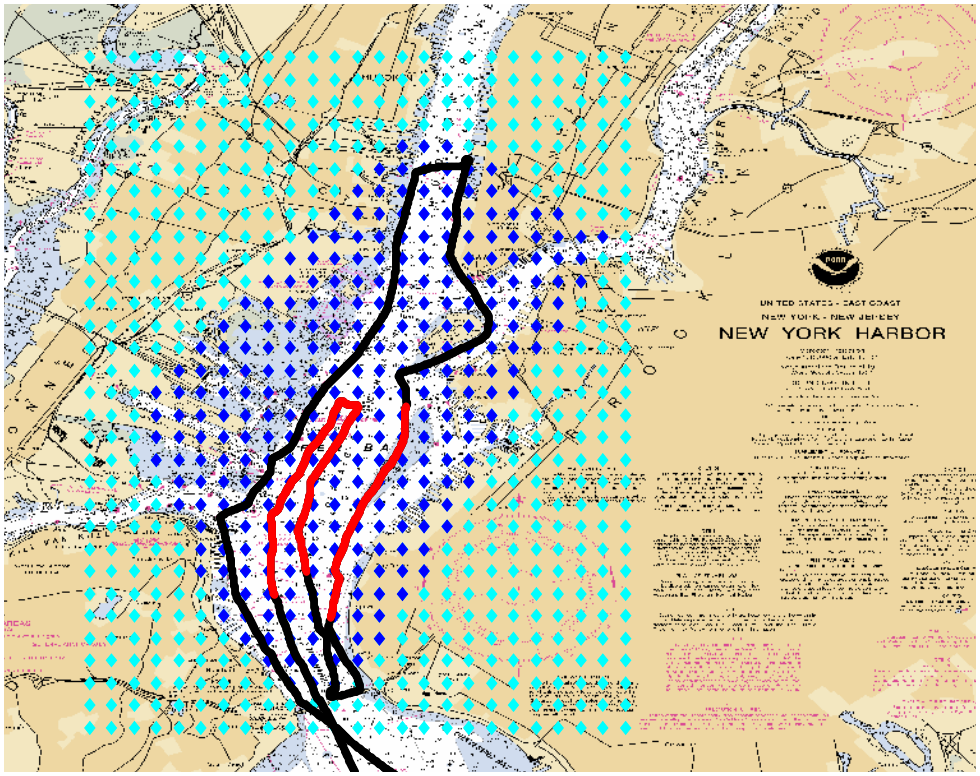


**Figure 16 – Coverage of the Delaunay ASF surface (dark blue dots) on the uniform grid (light blue dots). Vessel track in black with portions used for analysis in red.**

To assess the quality of these interpolated static grids, we recomputed the Loran positions for two portions of one of the slow circuits of the upper harbor (shown in red in Figure 16 – these stretches were chosen as being in the center of our grid area, away from bridge structures that might impact performance). Specifically, we took the measured Loran TOAs along those tracks, removed a spatial ASF estimate at each point based on interpolating the grid, removed the temporal component estimated at Staten Island, computed the Loran position, and compared the result to the GPS position. The absolute position error versus time of day (in hours) along the track appears in Figure 17. In this figure, green marks the Loran performance; the magenta line shows the desired performance of 20 meters. To better assess the results of this test, we computed some statistics; Figure 18 shows the histogram of the position error and its corresponding cumulative distribution function (cdf). We note that the 95% performance was 26 meters; not good enough for HEA applications. We expect that the wide spacing of the static measurements accounts for much of this error.

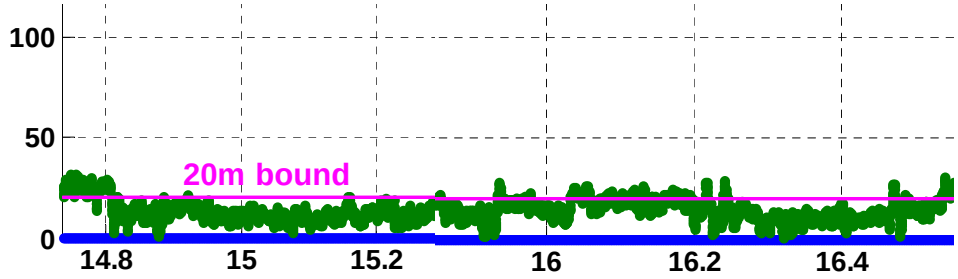


**Figure 17 – Typical performance of the static ASF grid.**

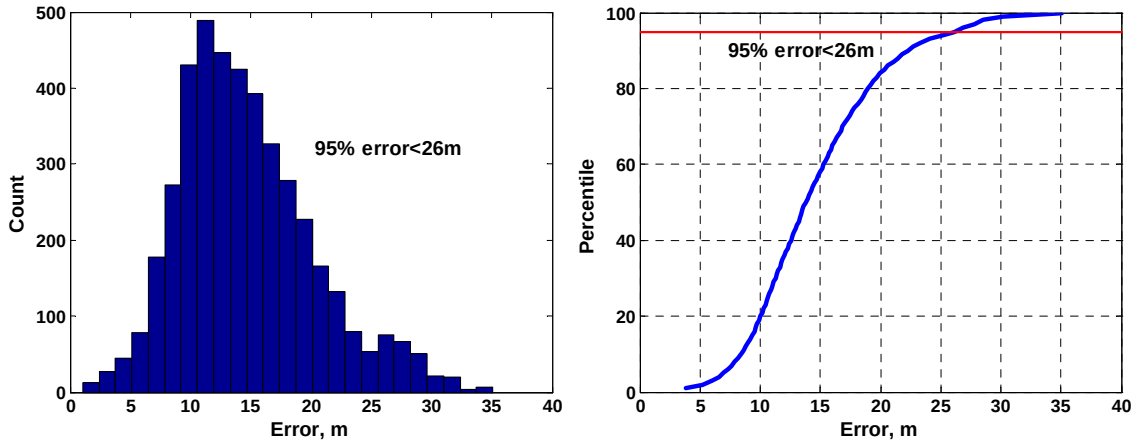


**Figure 18 – Statistics of the static grid performance.**

## *Grid Creation – Dynamic Data*

The primary purpose of this work was to mitigate the limitations of our Jan 2005 effort on the Thames River. While we cannot solve the missing data problem, we have developed a method based on standard bilinear interpolation that widens (doubles in both latitude and longitude) the area in which data impacts a grid value, that results in correlated ASF values on adjacent grid points, and employs the geometric position of the measurement relative to the grid point in the estimation method.

To understand the method, first recall the development of standard linear interpolation:

> *Given the values of a two-dimensional function F(x,y) at rectangularly spaced grid points, $x_j$ and $y_k$, we can estimate its value at an arbitrary location x,y by*
>
> $$\begin{aligned} F(x,y) \quad = \quad & (1-a)(1-b)F(x_j,y_k) + a(1-b)F(x_{j+1},y_k) \\ & + b(1-a)F(x_j,y_{k+1}) + abF(x_{j+1},y_{k+1}) \end{aligned}$$
>
> *in which $x_j \le x < x_{j+1}$ , $y_k \le y < y_{k+1}$, and a and b are defined by*
>
> $$a = \frac{x - x_j}{x_{j+1} - x_j} \quad \text{and} \quad b = \frac{y - y_k}{y_{k+1} - y_k}$$

In the general formulation, *a* and *b* are the relative horizontal and vertical position of the desired point *x,y* within the rectangular formed by the two closest values of $x_j$ and $y_k$ (see Figure 19). Bilinear interpolation first forms the pair of parallel horizontal (or vertical) line segments connecting the values of the function at these adjacent grid values, linearly interpolating each in *x* (or *y*), next forms the single vertical (horizontal) line connecting those two interpolated values, and finally interpolates on that line for the desired *y* (or *x*) value.

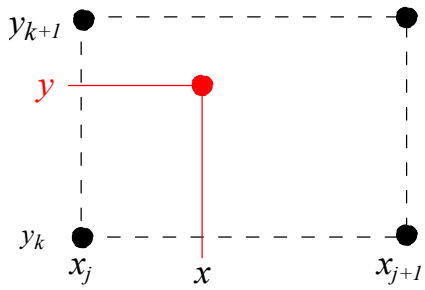


**Figure 19 – Example of standard bilinear interpolation.**

Viewed from afar, interpolation is the reverse of our situation – interpolation requires the values at the grid points and finds the value at an arbitrary point while we have the values at (potentially) many arbitrary points and wish to find the values at grid points. To solve our problem, then, we turn the interpolation equation around yielding

$$\begin{aligned} & (1-a)(1-b)F(x_j,y_k) + a(1-b)F(x_{j+1},y_k) \\ & + b(1-a)F(x_j,y_{k+1}) + abF(x_{j+1},y_{k+1}) \quad = \quad F(x,y) \end{aligned}$$

We interpret this as a linear equation in four unknowns (the values of *F* at the four grid points); the coefficients (depending upon *a* and *b* which are functions of the vessel location, from GPS) and the measurement *F*(*x,y*) are all known. Taking multiple measurements (at least 4) at distinct locations within the rectangle bounded by the four grid points yields sufficient simultaneous equations to enable a solution. Since we expect that the measurements (each ASF) are noisy, we prefer to take many data points and implement a least squares solution to the resulting set of over determined linear equations.

This “inverse interpolation” scheme addresses several of the limitations of our previous work on grid development:

- Some ASF grid values are missing – while we can still suffer from this problem, measurements now play a role in four grid points, effectively doubling the density of grid points (or quadrupling the number of measurements used in a grid value estimate). For example, the center grid value in Figure 20 is solved for using all of the track points marked in green, not just those closer to that grid point than some other.

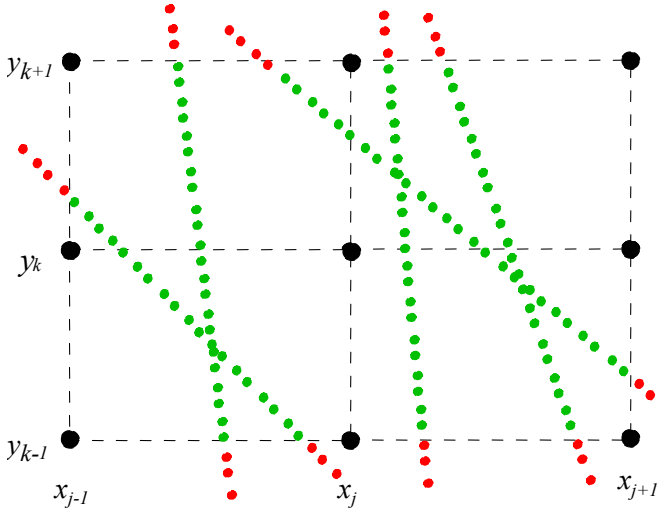


**Figure 20 – Example of inverse bilinear interpolation.**

- Since each measurement is employed in solving for 4 grid points and adjacent grid points share common measurements (with different coefficients in the linear equations), there is now an explicit correlation of the ASF value at adjacent grid points. For example, the green points in the top right rectangle in Figure 20 are in the equations for the center grid point as well as those of the top center and middle right grid points
- The relative location of the data directly impacts the resulting grid values through the values of *a* and *b* in each simultaneous equation.

An example of solving for the grid from dynamic data for Loran station Nantucket appears in Figure 21 for a grid point spacing of 0.005 degrees, both Latitude and Longitude. The coverage of this grid appears in Figure 22 (again, as in Figure 16, light blue shows the full grid and dark blue the inverse interpolation grid). When comparing these results to that of the Delaunay grid in Figure 15 and Figure 16, this result looks quite sparse and limited. This is indeed so since only the on-the-water data from Figure 5, Figure 6, and Figure 7 are included in the calculation (the on-the-water static points are just a very *slowly* moving vessel). While we could include the on-the-land points as well, the fact that they fall far from any other data would result in measurements clustered in one interpolation rectangle. Since such limited spread typically produces poor solutions of the equations, and hence poor estimates of the ASFs, we ignore those here. Further, the inverse interpolation solutions at the edges of the range of data generally overcompensate in the estimates (not having any data on the other side); hence, we erode the resulting grid region slightly to produce a cleaner set of values. And finally, while theoretically we could set the grid spacing at any value, the spread of points in the tracks from New York harbor limit us to grids of approximately 500 meters or larger. Smaller spacing results in

interpolation cells without data and, hence, poor estimates as noted above. We are currently planning more extensive on-the-water surveying of the Thames River harbor and expect to report on the effects of inverse interpolation grid size in future publications.

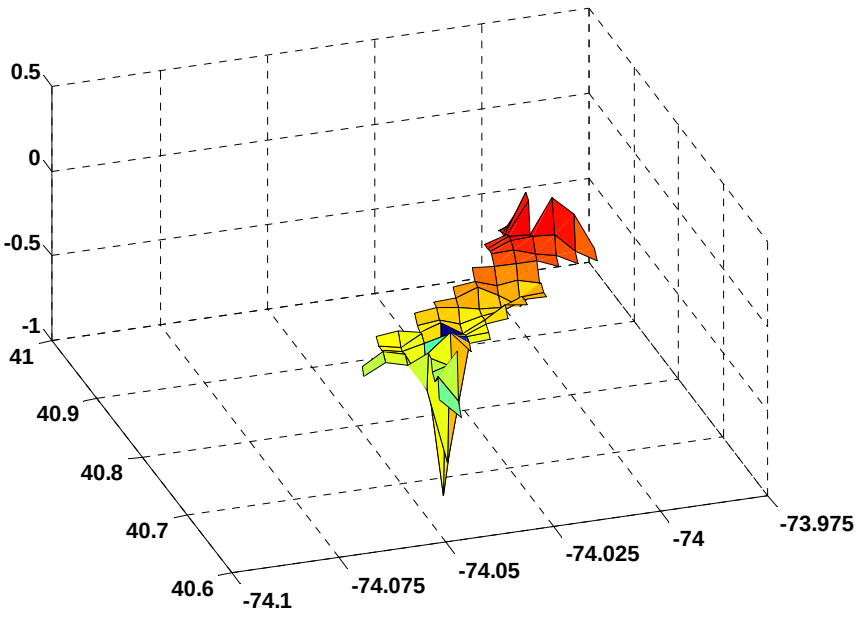


**Figure 21 – The inverse interpolation ASF grid for Nantucket.**

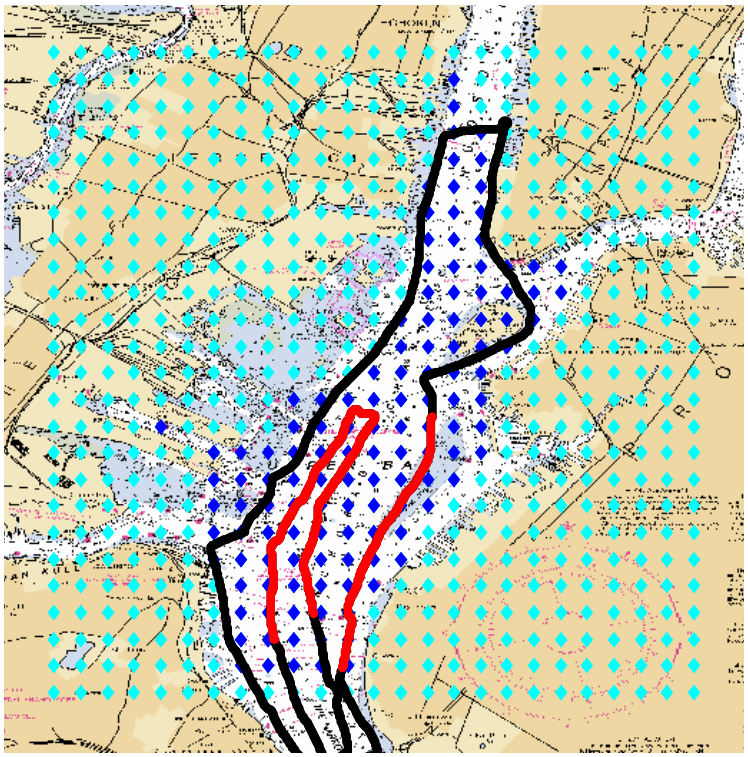

**Figure 22 – Coverage of the inverse interpolation ASF grid.**

To assess the quality of these interpolated dynamic grids, we first repeat the experiment described above for static grids (the red track in Figure 22 which is the same track used previously). The absolute position error versus time of day (in hours) along the track for the dynamic grids appears in Figure 23; green marks the Loran performance, magenta the desired 20 meters. The statistics of this test appear in Figure 24. In this case the 95% performance was less than 15 meters; good enough for HEA applications.

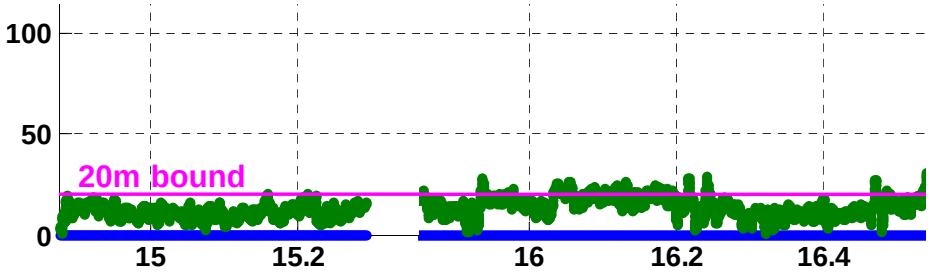


**Figure 23 – Typical performance of the dynamic ASF grid.**

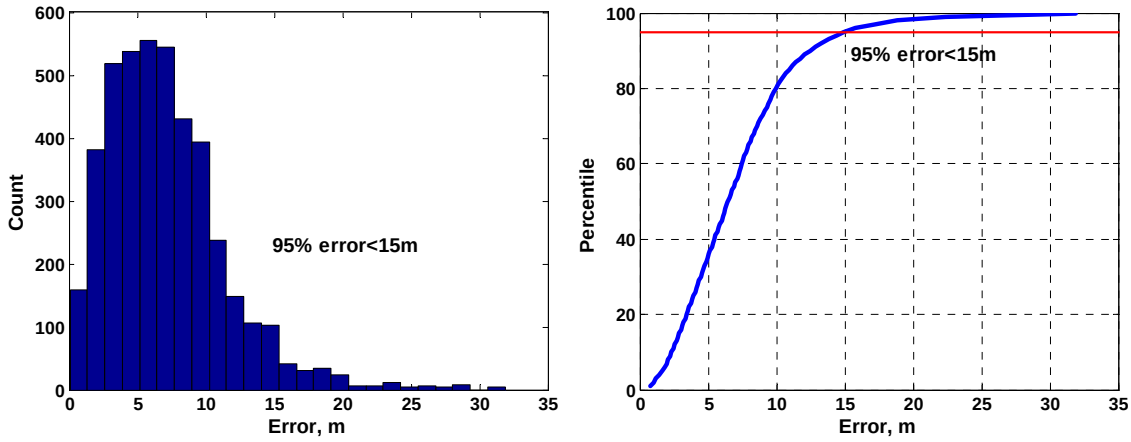


**Figure 24 – Statistics of the static grid performance.**

As a second test of the inverse interpolation grids, we considered a track in the lower harbor (shown in red in Figure 25). Specifically, we developed ASF grids based upon part of the data set traversing the center and edges of the channel. Using the same convention as before, the dark blue triangles in Figure 25 show where grid values exist, the light blue are grid points on the uniform grid for which no data was available. We then processed TOAs from a separate track (from a different day, not used in the grid development) to assess Loran position performance. The absolute position error appears in Figure 26; the statistics in Figure 27. In this case the 95% performance was less than 10 meters!

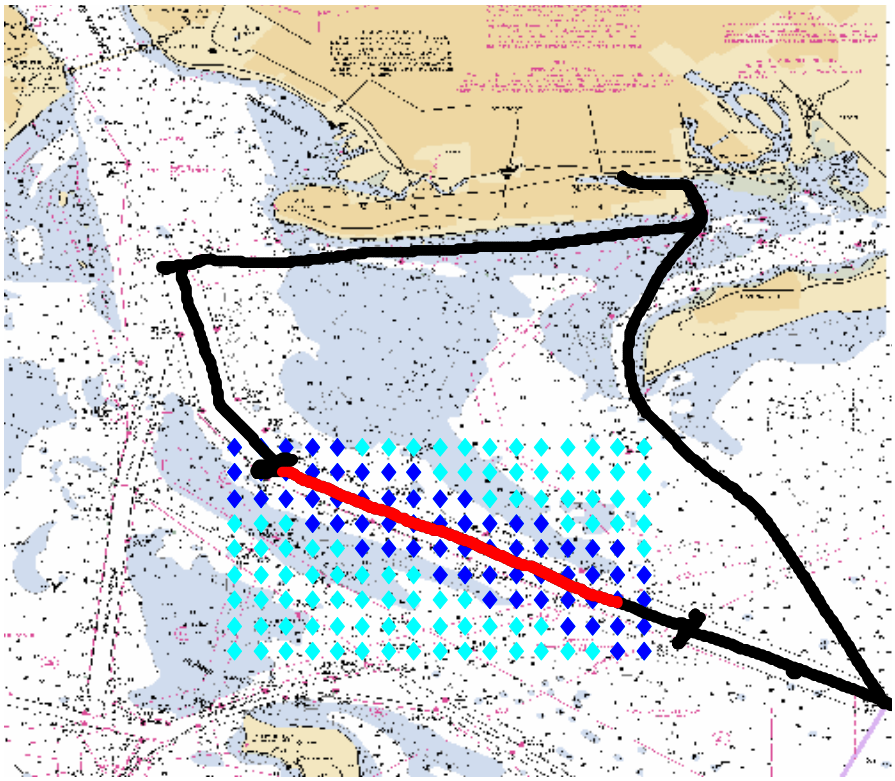

**Figure 25 – Lower harbor test: grid from one day and track from another.**

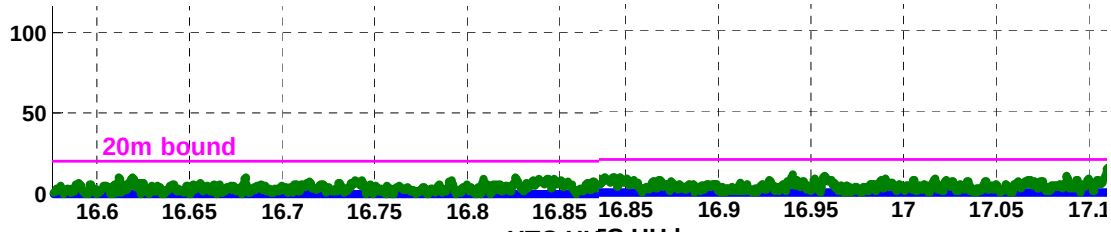


**Figure 26 – Error performance of the lower harbor test.**

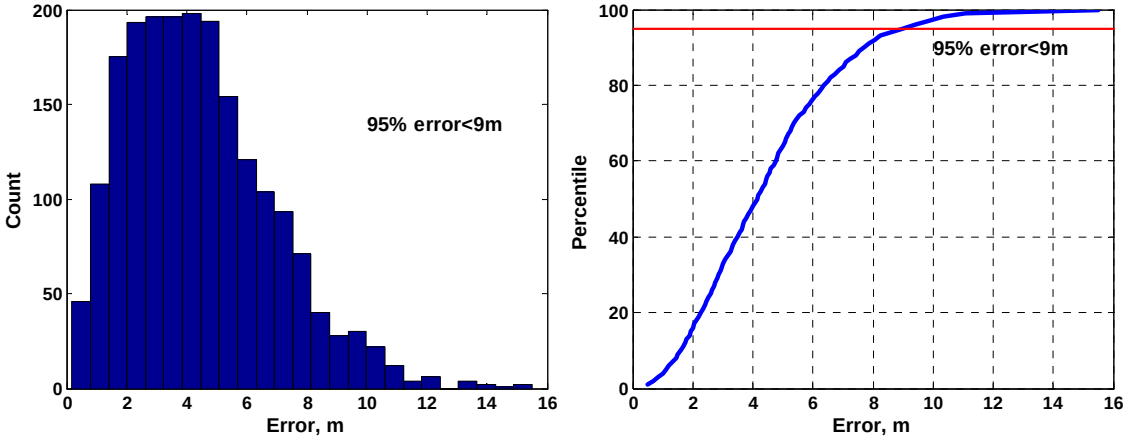


**Figure 27 – Statistics of the lower harbor test.**

## Conclusions/Future

After reviewing some prior work on ASF grid computation, we have introduced the inverse interpolation method which employs the precise position of survey data and adds correlation across the grid estimate. Further, we demonstrated that such grids can achieve the desired HEA performance level of sub-20 meter accuracy using a 500-meter grid. Open questions still exist on the required density of the grid and the number of data points necessary (per grid cell) to get reliable ASF estimates.

Currently, we are involved in resurveying the Thames River area to attempt to answer the above questions. The computed ASF grids, and the results of a live test of navigating with the grids, will be described in early 2007.

## Acknowledgments

The authors would like to recognize the support of the the Alion team (C. Oates, M. Wiggins, K. Dykstra, M. Kuhn), the Loran ASF Working Group (K. Bridges, S. Lo, P. Morris, D. Diggle, G. Johnson, P. Swaszek, T. Gunther, R. Wenzel, and J. Carroll), and LT Dave Lown of the USCG Loran Support Unit who is the sponsor of this work.

## Disclaimer and Note

The views expressed herein are those of the authors and are not to be construed as official or reflecting the views of the U.S. Coast Guard, Federal Aviation Administration, or any agency of the U.S. Government.

## References

[1] "LORAN-C User Handbook," United States Coast Guard, Washington, DC COMDTPUB P16562.6, 1994.

[2] M. Kuhn, G. Johnson, P. Swaszek*, et al.*, "Warping Time and Space: Spatial Correlation of Temporal Variations," presented at the 35th Annual Technical Symposium, International Loran Association, Groton, CT, 24-25 October 2006.

[3] R. Hartnett, G. Johnson, and P. Swaszek, "Navigating Using an ASF Grid for Harbor Entrance and Approach," presented at the Institute of Navigation, Annual Meeting, Dayton, OH, 6 - 9 June 2004.

[4] P. Swaszek, G. Johnson, R. Hartnett*, et al.*, "Airport ASF Mapping Methodology Update," presented at the 34th Annual Technical Symposium, International Loran Association, Santa Barbara, CA, 18-19 October 2005.

[5] G. Johnson, P. Swaszek, R. Hartnett, and R. Shalaev, "Performance Trials of an Integrated Loran/GPS/IMU Navigation System, Part I," presented at the Institute of Navigation, National Technical Meeting, San Diego, CA, 24 - 27 January 2005.

[6] N. A. C. Cressie, *Statistics for Spatial Data*: Wiley Interscience, 1991.